LANGMUIR

Article

pubs.acs.org/Langmuir

Unraveling the Mystery of Stöber Silica's Microporosity

Shanshan Li,[†,‡,§] Quan Wan,[*,†] Zonghua Qin,[†] Yuhong Fu,[†,‡] and Yuantao Gu[†,‡]

[†]State Key Laboratory of Ore Deposit Geochemistry, Institute of Geochemistry, Chinese Academy of Sciences, Guiyang, Guizhou 550081, China

[‡]University of Chinese Academy of Sciences, Beijing 100049, China

[§]School of Chemistry and Materials Science, Guizhou Normal University, Guiyang, Guizhou 550001, China

Supporting Information

ABSTRACT: Puzzling aspects of the microporous structure of Stöber silica, including inconsistencies in the BET specific surface area and the long measurement time required for N_2 adsorption, hinder further research on and potential applications of this material. In this work, Stöber silica samples prepared using systematic and detailed post-treatment methods were characterized by N_2 adsorption, scanning electron microscopy, transmission electron microscopy, inductively coupled plasma optical emission spectrometry, elemental analysis, and Fourier transform infrared spectroscopy. We have found that the often overlooked sample preparation conditions may be the main causes that perplex the gas adsorption characterization results of Stöber silica samples. The pore-blocking processes associated with a variety of sample treatment methods are discussed in detail. Strong evidence for the particle growth model and pore-blocking mechanism involving ethoxyl groups, Si species, and condensation of silanols is provided. A remarkable result is that the measurement time is shortened from 1 month in our previous work to 2−3 days for samples with large specific surface areas. A suitable post-treatment condition is recommended to obtain microporous Stöber silica with a short measurement time, including water washing, low temperature drying without a vacuum, and a short storage time.

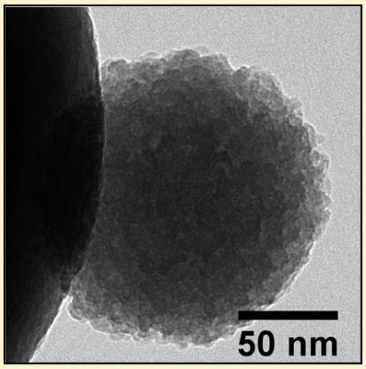

1. INTRODUCTION

The Stöber process is well-known for the production of almost perfectly spherical silica particles with a monodisperse size distribution.[1] Due to its unique external features, Stöber silica has been widely used in the preparation of various functional materials, including yolk−shell nanostructures and high-quality photonic crystals.[2,3] Stöber silica has also been selected as a model material in studies of the particle size effects on the rate of silica dissolution and control of surface silanol density.[4−6] Therefore, previous studies have often focused on controlling the size and monodispersity of Stöber silica particles.[7−10] However, in many processes, the internal porous structure must be recognized, and the corresponding specific surface area (SSA) is an essential parameter. For example, the SSA was often used as a normalizing parameter in the calculation of both the dissolution rates of Stöber silica particles and surface group densities. Additionally, because many fundamental mineralogical and geochemical processes were found to be associated with nanoporous structures,[11−14] Stöber silica might serve as an excellent micropore model in relevant mechanistic studies. All of these studies require a clear understanding of Stöber silica's internal porous structure and its pore formation mechanism.

However, considerable inconsistencies and contradictions were reported in the literature with respect to Stöber silica's porosity. The SSA measured from conventional nitrogen adsorption (N_2, 77 K) varied over a wide range (from several m^2/g to several hundred m^2/g) even when the synthetic conditions were similar.[15] Compared with the geometric SSA, the measured SSA at times showed a porous structure, but at other times, it indicated a nonporous structure (see Table 1).[6,15−21] Similarly, many methods, such as pycnometry, acid−base titration, liquid-phase adsorption, and small-angle X-ray scattering, characterized Stöber silica as a porous structure.[15,17,22−24] Although certain researchers reported that this material displayed a gel-like surface structure or the activated diffusion effect, in which temperature promotes entry of the adsorbate in narrow sections of micropores,[17] to the best of our knowledge, a commonly accepted explanation has not been suggested until now. The tremendous differences in SSA values might lead to severely misleading interpretations of Stöber silica's surface and internal properties. For example, the surface silanol group density calculated from the SSA combined with thermogravimetric data varied over a wide range (5.7−56 OH/nm^2),[6] which was far from the commonly accepted surface silanol group density of amorphous silica (4−5 OH/nm^2).[25] Wang also pointed out that one study indicated an opposite trend for the dissolution rate when normalized to the SSA.[11] Thus, it is important to identify the reason for the tremendous differences in SSA values and reveal the mysterious and puzzling internal structure of Stöber silica.

Received: July 4, 2016
Revised: August 19, 2016
Published: August 22, 2016

DOI: 10.1021/acs.langmuir.6b02472
Langmuir 2016, 32, 9180−9187

Table 1. Discrepancies on Stöber Silica's Porosity as Exemplified by Gas Adsorption Results

	samples indicating low porosity				samples indicating high porosity			
diameter of particle (nm)	250	270	335	570	42	500	670	730
SSA (m^2/g)[a]	12.5	18.0	10.0	7.6	369.0	144.0	324.0	240.0
S_G (m^2/g)[b]	10.9	10.1	8.1	4.8	64.9	6.3	4.1	3.7
reference	16	17	18	6	19	20	21	15

[a] The SSA from the literature was calculated using the BET method. [b] The S_G denotes the geometrical specific surface area, and was calculated using the diameter of the particles and the density of 1.9 g/cm^3.

Table 2. Representative Sample Coding Based on Reaction Time and Post-Treatment Conditions

sample	reaction temperature (°C)	reaction time (min)	washing solvent[a]	washing times	drying temperature[b] (°C)	drying time (h)
S80-N-50	20	80	N		50	2
S80-E10-50	20	80	E	10[c]	50	2
S80-HW10-50	20	80	HW	10	50	2
S80-E5+HW5-50	20	80	E+HW	5 + 5[d]	50	2
S80-W10-50	20	80	W	10	50	2
S80-W10-120−200	20	80	W	10	120−200	2
S80-W4-50	20	80	W	4	50	2
S80-W4-120	20	80	W	4	120	2
S80-W4-RT−120	20	80	W	4	RT−120	2
S80-W4-120−200	20	80	W	4	120−200	2
S80-W4-200	20	80	W	4	200	2
S80-W4-200V[e]	20	80	W	4	200V	2
S80-W4-50V	20	80	W	4	50V	2
S80-W4+E4-50	20	80	W+E	4 + 4	50	2
S80-W4+E4+W4-50	20	80	W+E+W	4 + 4 + 4	50	2
S80-W2-50	20	80	W	2	50	2
S180-W4-50	20	180	W	4	50	2
S180-W4-RT−120	20	180	W	4	RT−120	2

[a] Washing solvent coding: N denotes absence of washing, E denotes ethanol, HW denotes hot deionized water, and W denotes deionized water. [b] Drying temperature coding: 50 denotes direct drying at 50 °C, 120−200 denotes heat drying from 120 to 200 °C for 2 h, RT−120 denotes heat drying from room temperature to 120 °C for 2 h, etc. [c] 10 denotes washing with ethanol 10 times. [d] 5 + 5 denotes washing with ethanol 5 times plus washing with hot deionized water 5 times, etc. [e] 200V denotes vacuum drying at 200 °C, and 50V denotes vacuum drying at 50 °C.

In the experiments in our previous work,[26] we demonstrated that the often overlooked post-treatment methods significantly influenced the SSA of Stöber silica as measured by N_2 adsorption at 77 K, such as reaction time, washing solvents, and drying temperature. The SSA of synthesized samples varied from 11.3 to 309.7 m^2/g with different post-treatment methods. Our results confirmed the existence of micropores formed by the aggregation of nuclei (from the initial nucleation process). In addition, we proposed pore-blocking mechanisms to explain the variation of their internal structures with post-treatment methods, which involved blocking by ethoxyl groups, TEOS monomers or oligomers (from hydrolysis and polymerization of tetraethyl orthosilicate) and condensation of silanols. Although we acquired samples with different SSA values by adjusting the post-treatment methods, the long duration required for N_2 adsorption measurement (approximately 1 month) for samples with large SSA (e.g., for samples with 309.7 m^2/g SSA) was a serious problem. The long measurement time meant that equilibrium was difficult to reach and might lead to inaccuracy of the analysis results, which significantly affects the application of and research on Stöber silica. The long measurement time for Stöber silica has also been reported in the literature,[15,27] but no commonly accepted explanation has been offered until now.

With many repetitions (>200 times) of the N_2 adsorption experiment, we recognized the sophisticated and subtle structure of Stöber silica, and as a result, we focused on the post-treatment methods in a systematic and detailed manner. In this study, we found that, in addition to the above-mentioned factors, the drying method (direct drying and heat drying), storage time, washing times, etc., also substantially influenced the N_2 adsorption results. The pore-blocking and particle-growth mechanisms were reinforced by strong evidence (ICP-OES, TEM, etc.). We elaborated the mechanisms of the pore structure evolution in the post-treatment processes, which helped unravel the mysteries on Stöber silica's subtle internal structure. This study also offers practical guidance on the synthesis of Stöber silica with large SSA for multiple research areas and applications.

2. EXPERIMENTAL SECTION

2.1. Materials. Tetraethyl orthosilicate (TEOS, 96%) was obtained from TCI (Shanghai, China) and used without further purification. Ethanol (99.7%) was sourced from Sinopharm Chemical Reagent Company, China. Ammonia (~26.5%) was purchased from Chongqing Chuanjiang Chemical Reagent Company, China. Deionized water was obtained from a Millipore synergy UV system and had a resistivity of 18.2 MΩ·cm.

2.2. Synthesis Process. Ammonia, deionized water, and ethanol were mixed in a flask and stirred at 20 °C for approximately 45 min (the temperature was controlled by a refrigerated-heating circulator), which was assumed to be sufficient to minimize compositional and temperature inhomogeneity in the mixture. Subsequently, a certain amount of TEOS was quickly added to the mixture, which was continuously stirred for an additional reaction period. The molar concentration of TEOS, NH_3, and H_2O was approximately 0.25, 0.5, and 7.5 M, respectively, assuming that all mixed liquid volumes were additive. To avoid possible effects of reaction volume, the total mixture volume was maintained at 80 mL in each batch. The reaction time for the process was controlled to 80 or 180 min. After reaction, the suspension was centrifuged at 10,000 rpm (9940 g) with a fixed-angle centrifuge to collect the precipitate of silica particles.

2.3. Post-Treatment of Synthesized Product. The collected silica product was post-treated using different processes. First, the product was washed with different washing solvents (deionized water, hot deionized water, ethanol, ethanol plus hot deionized water, etc.) and different washing times. Specifically, for each washing cycle, 10 mL of washing solvent was used to wash the collected product from 40 mL of suspension. Each washing cycle was conducted using a vortex mixer for 2 min, and the suspension was subsequently centrifuged and separated by decanting the supernatant liquid. After washing, the samples were dried at 50, 120, or 200 °C for 2 h in an oven. Two different drying methods were used, including direct drying by placing the samples in an oven at the target temperature and heat drying by placing the samples in a room temperature oven and heating to the target temperature. After drying, the samples were stored for no more than 3 days prior to measurement by N_2 adsorption at 77 K to eliminate the influence of the long storage time. Thus, the precipitate of each batch was treated with two to three different methods, and two to three samples were acquired. The detailed processing conditions for the representative samples are summarized in Table 2. The sample coding includes three hyphenated segments. The first segment denotes the reaction time (min), followed by the second segment that indicates the washing solvents and washing times, and the third segment denotes the drying temperature and drying methods. For example, S80-E10-50 denotes a sample with 80 min of reaction time, 10 washes with ethanol, and direct drying at 50 °C for 2 h. S80-W10-120−200 denotes a sample with 80 min of reaction time, 10 water washes, and heat drying from 120 to 200 °C (product placed in an oven at 120 °C and heated to 200 °C) for 2 h.

2.4. Characterization of Post-Treated Samples. Scanning electron microscopy (SEM) images were obtained on a JEOL JSM-7800F (Japan) instrument to analyze the sizes and shapes of the Stöber silica particles. Transmission electron microscopy (TEM) measurements were performed on an FEI Tecnai G2 F20 instrument to investigate the internal microscopic structures of the particles.

Nitrogen adsorption (77 K) was performed using an Autosorb-iQ$_2$-MP gas adsorption analyzer (Quantachrome, USA). Prior to measurement, the samples were outgassed at 200 °C for 12 h under a vacuum. The N_2 (0.162 nm^2 molecular cross-sectional area) is of 99.999% purity, and the p/p_0 ranged from 10^{-6} to 0.99. BET (Brunauer−Emmett−Teller) and NLDFT (nonlocal density functional theory) models were used to analyze the specific surface area, pore size, pore volume, etc. The relative pressure range of BET was automatically chosen by the Micropore BET Assistant in the Quantachrome software. For samples with large SSA, the relative pressure range was about 0.005−0.075 p/p_0, and the relative range was about 0.13−0.28 p/p_0 for nonporous samples. For the NLDFT analysis, the whole relative pressure range was chosen.

The silicon contents of the supernatant liquid after washing were measured via inductively coupled plasma optical emission spectrometry (ICP-OES, VISTA-MPX, Varian). The solutions were centrifuged at 10,000 rpm for 20 min to remove the residual silica particles.

The elemental contents (carbon and nitrogen) were measured using an elemental analysis instrument (Vario MACRO cube, Elementar Analysensysteme GmbH, Germany). The result for each sample (20−50 mg) was the average value of two measurements.

The FTIR transmission spectra were determined using a Fourier transform infrared spectrometer (Vertex 70, Bruker, Germany). For each sample, 16 scans in the spectral range 4000−400 cm^{-1} were recorded with a resolution of 4 cm^{-1}.

3. RESULTS AND DISCUSSION

3.1. Characterization of the Stöber Silica Samples.

SEM micrographs of two representative Stöber silica samples are shown in Figure 1 (samples S80-W10-50 and S80-N-50). All particles display regular spherical shapes and good size monodispersity. The diameter of the samples with a reaction time of 180 min (∼200 nm) is slightly larger than the diameter of the samples with a reaction time of 80 min (∼185 nm), indicating that, after 80 min of reaction, the particles continue to grow at a slow rate. According to the SEM micrographs, regardless of the washing solvents used, the washing process had no obvious effect on the morphology and size of the particles.

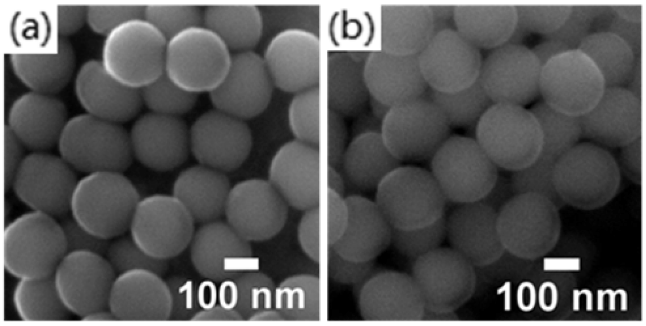

Figure 1. SEM micrographs of representative samples: (a) sample S80-W10-50; (b) sample S80-N-50.

The adsorption isotherms for samples subjected to water washing (including hot water washing) and 50 °C direct drying (such as samples S80-E5+HW5-50, S80-W10-50, S80-HW10-50, etc.) are classified as type I (according to IUPAC classification), indicating a microporous structure (see Figure 2 for sample S80-W10-50). The dramatic increase in the adsorption volume at $p/p_0 > 0.97$ is ascribed to filling of nitrogen molecules in the interparticle pores. Samples washed with ethanol and without washing (samples S80-E10-50 and S80-N-50) display a type II isotherm typical of a nonporous material (Figure S1 shows the isotherm and pore size distribution of sample S80-E10-50). The results of gas adsorption analysis (based on the BET and NLDFT models) including the specific surface area, pore size, pore volume, etc., for representative samples are summarized in Table 3. The samples subjected to water washing and 50 °C direct drying have an SSA of >310 m^2/g and a microporous volume of approximately 0.1 cc/g. The pore size distribution for these samples shows two peaks located at 0.8 and 1.1 nm in the NLDFT, and the higher point is shown in Table 3, i.e., 1.1 nm of sample S80-W10-50 (Figure 2b). The microporous volumes of samples S80-E10-50 and S80-N-50 are negligible, and their SSA values are much smaller than those of samples subjected to water washing.

Certain samples require a long time to achieve equilibrium during measurement (such as samples S80-W4-RT−120, S80-W4-120−200, etc.), up to 1 month in our previous work, and thus, it was difficult to finish all measurements. Therefore, we set a criterion that, after 3 days of measuring, the measurement would be stopped if the p/p_0 remained below 10^{-3}. These unfinished samples could aid in understanding the variation of Stöber silica's microporous structure with post-treatment conditions, and accordingly, the measurement times and sample masses of all samples are listed in Table 3 for comparison. The measurement time (obtained from the instrument testing software) was updated only after an adsorption data point was acquired, which suggests that the

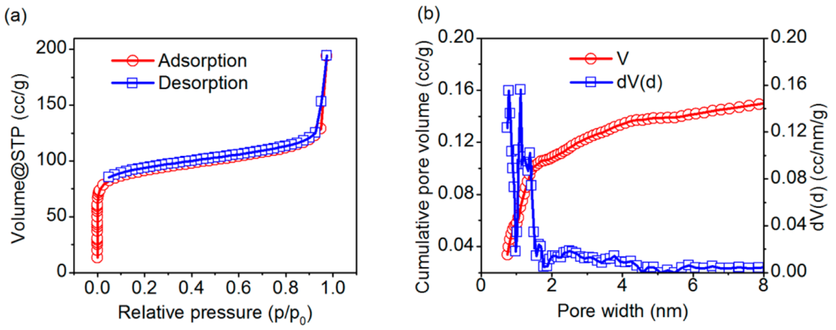

Figure 2. (a) Gas adsorption (N_2 at 77 K) isotherm of sample S80-W10-50 and (b) pore size distribution of sample S80-W10-50 from NLDFT.

Table 3. Measurement Parameters and Analysis Results of Gas Adsorption for Representative Samples

			NLDFT					
sample	sample mass (mg)	S_{BET} (m^2/g)[a]	model type[b]	surface area (m^2/g)	pore width (nm)	pore volume (cc/g)	micropore volume (cc/g)[c]	measuring time (h:min)
S80-N-50	55.8	53.8	III	61.1	0.8	0.056	0.005	29:58
S80-E10-50	61.7	47.8	III	37.5	3.5	0.055		46:56
S80-HW10-50	51.9	351.8	III	555.3	1.1	0.195	0.105	36:26
S80-E5+HW5-50	55.8	311.5	III	487.0	1.1	0.178	0.092	59:06
S80-W10-50	62.9	344.3	III	564.0	1.1	0.186	0.108	41:08
	62.2[d]	360.6	III	603.0	1.1	0.190	0.115	44:07
S80-W10-120–200	61.9	315.6	III	495.2	1.1	0.174	0.098	78:20
S80-W4-50	47.5	357.1	III	502.6	0.8	0.188	0.104	34:47
S80-W4-120	65.1		$p/p_0 \sim 2.4 \times 10^{-5}$, $V \sim 20.0$ cc/g					56:58
S80-W4-RT–120	66.2		$p/p_0 \sim 2.4 \times 10^{-5}$, $V \sim 14.7$ cc/g					71:27
S80-W4-120–200	63.8		$p/p_0 \sim 2.4 \times 10^{-5}$, $V \sim 22.8$ cc/g					79:45
S80-W4-200	63.7		$p/p_0 \sim 2.4 \times 10^{-5}$, $V \sim 22.6$ cc/g					78:59
S80-W4-200V	64.8		$p/p_0 \sim 2.0 \times 10^{-4}$, $V \sim 36.0$ cc/g					74:12
S80-W4-50V	76.2	64.3	III	82.2	0.8	0.061	0.010	28:48
S80-W4+E4-50	60.6	305.3	III	488.0	0.8	0.178	0.092	87:35
S80-W4+E4+W4-50	58.1	346.6	III	482.2	0.8	0.177	0.107	34:33
S80-W2-50	52.1	342.5	III	486.7	0.8	0.183	0.099	36:29
S180-W4-50	55.7	321.3	III	523.6	1.1	0.186	0.092	51:08
S180-W4-RT–120	65.8		$p/p_0 \sim 2.1 \times 10^{-4}$, $V \sim 4.8$ cc/g					64:44

[a] Specific surface area calculated using the BET model. [b] NLDFT offers three types of models for silica. Type I: cylinder pore, NLDFT adsorption branch model. Type II: cylinder pore, NLDFT equilibrium model. Type III: cylinder/sphere pore, NLDFT adsorption model. The fitting error of the type III model for most samples is the minimum value. [c] Micropore volume is the volume for pore sizes of less than 2 nm. [d] Denotes outgassing at 100 °C for 0.5 h and at 120 °C for 12 h; all other samples outgassed at 100 °C for 0.5 h and 200 °C for 12 h.

actual measurement time of certain unfinished samples might be larger than that recorded in Table 3.

3.2. Effect of Washing Solvent.

In our previous work,[26] we postulated that the aggregation plus monomer addition model could reasonably describe the growth process of Stöber silica; i.e., nuclei aggregate to form larger particles, and the micropores inside the particles are interparticle pores of the nuclei. At the same time, the addition of monomers or oligomers to the particle surface occurs and becomes the dominant process during the late growth period, and thus, the micropore entrances or channels might become blocked during the addition process. We also suggested water as the preferred washing solvent and proposed two pore-blocking mechanisms (by ethoxyl groups and TEOS monomers or oligomers) to explain the variation in the SSA. In this section, more detailed evidence is offered to affirm the pore-blocking mechanisms and particle growth model.

First, the elemental analysis results (the C and N contents are listed in Table 4 for selected representative samples) show that water washing could clear the residual ethoxyl groups (OC_2H_5, from incomplete hydrolysis of TEOS), but ethanol washing might lead to a complicated or blocked pore structure. For example, the carbon contents of the samples washed 4 times with water (0.02%) or 10 times with hot water (0.04%) are much smaller than those of the samples without washing (0.85%). The residual ethoxyl groups on the particle surfaces were hydrolyzed and converted into silanol groups (OH) (see eq S1 in the Supporting Information) during water washing, which might clear the pore entrances or channels to a certain extent because the size of the silanol group is smaller than that

Table 4. Carbon and Nitrogen Contents of Selected Representative Samples

sample	carbon (wt %)	nitrogen (wt %)
S80-N-50	0.85	1.92
S80-E10-50	2.79	1.50
S80-W4-50	0.02	1.00
S80-W4-120	0.05	0.09
S80-W4-RT–120	0.06	0.08
S80-W10-50	0.18	0.80
S80-HW10-50	0.04	0.24

of the ethoxyl group. At the same time, the FTIR transmission spectrum (see Figure S2 in the Supporting Information) also indicates the removal of carbon through water or hot water washing. According to the literature, silica can be esterified by alcohols in the presence of NH_3.[28] The higher C content of sample S80-E10-50 (2.79%) than sample S80-N-50 (0.85%) suggests the occurrence of esterification. Accordingly, the pore structure might become complicated or blocked during ethanol washing due to conversion of the silanol group into an ethoxyl group. This process could aid in understanding why the SSA of sample S80-E10-50 (47.8 m^2/g) is slightly smaller than that of sample S80-N-50 (53.8 m^2/g).

Furthermore, after washing, we collected the supernatant liquid to measure the contents of Si species (mainly hydrolyzed monomers or oligomers) using ICP-OES, which were conventionally expressed as SiO_2 contents. The SiO_2 contents (see Figure 3) in the supernatant liquid after one wash with water or hot water are greater than 500 mg/L but less than the 15 mg/L with ethanol washing. As mentioned in our previous work,[26] water washing could effectively contribute to clearing of pore-blocking through hydrolyzing and removing the TEOS monomers or oligomers (see eq S2 in the Supporting Information). Thus, the SiO_2 contents in the supernatant liquid after water washing are much greater than those after ethanol washing. The contents of SiO_2 in the supernatant liquid (pH > 10) were compatible with the solubility of amorphous silica in the literature,[28] and similar results were reported in previous research.[29] During a 2 min wash, the monomers or oligomers attached to the entrances or channels of pores could be dissolved more easily than bulk silica due to their small size and loose structure. Although the contents of Si species decrease with washing time, the effect of the entire washing process is significant.

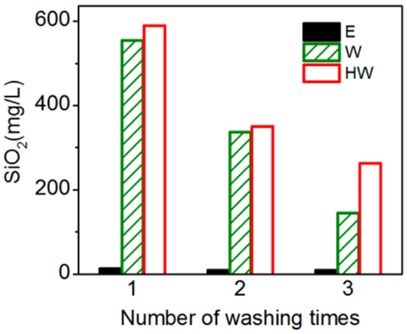

Figure 3. Concentrations of dissolved silica in liquid phases after successive washing with ethanol, water, and hot water (E, S80-E10-50; W, S80-W10-50; HW, S80-HW10-50).

According to these two sources of evidence, after water washing, the blocking pore entrances and channels were cleared such that the N_2 molecules could enter or diffuse more smoothly. To further elucidate the effect of pore-blocking by ethoxyl groups and monomers or oligomers, one sample was washed four times with water followed by four washes with ethanol (sample S80-W4+E4-50) and four more washes with water (sample S80-W4+E4+W4-50). The SSA of sample S80-W4+E4-50 was 305.3 m^2/g, and a longer time (approximately 88 h) was required to finish the measurement than sample S80-W4-50 (approximately 35 h), which suggests that, after ethanol washing, esterification indeed influences the measurement to a certain extent and results in a smaller SSA and longer measurement time. However, the extent of pore-blocking is obviously much smaller than that of sample directly washed with ethanol, which implies that the monomers or oligomers might be the dominant contributors to pore-blocking. As we expected, slight pore-blocking was cleared by continued water washing (sample S80-W4+E4+W4-50), and the sample displayed a large SSA and short measurement time, similar to sample S80-W4-50.

Moreover, we observed the microstructures of the samples using TEM. The TEM micrograph (Figure 4) shows that the particles are formed by aggregation of nuclei, which is strong evidence to support our aggregation plus monomer addition growth process and the pore-blocking mechanisms. It was very difficult to find the structure in Figure 4 in all samples (especially with large-size particles), because of TEM's inability to reveal the internal subtle structure of large particles. After many trials, we found such an aggregation structure in the sample that was similar to sample S80-W10-50 because it contains small particles, and we could observe the microstructure more easily.

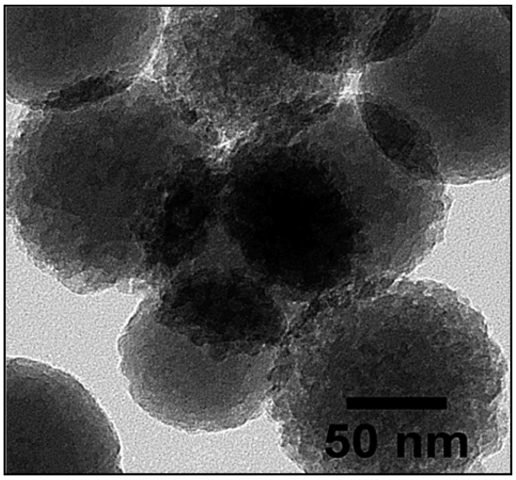

Figure 4. TEM micrograph of Stöber silica.

3.3. Effect of the Drying Conditions.

The drying conditions had a profound effect on SSA, and we discussed the influence of the drying temperature on the condensation of silanols in our previous work.[26] In this section, we investigate and discuss the influence of the drying temperature and drying method in additional detail.

According to Table 3, the samples subjected to water washing and direct drying at 50 °C (such as S80-W4-50, S80-HW10-50, S80-W10-50, etc.) exhibited large SSA values, and the measurement time was remarkably shortened from 1 month to 2−3 days. In addition, the isotherm desorption and adsorption branches overlap (see Figure 2a) compared with previous diverged branches due to disequilibrium associated with the long measurement time.[26] However, the measurement times for samples with water washing and drying at higher temperature (direct drying at 120 or 200 °C) were much longer (see samples S80-W4-120 and S80-W4-200 in Table 3), which suggests that, in addition to washing, the drying temperature conspicuously affects the microporous structure.

As shown in Table 4, the N content decreases drastically with increasing temperature, e.g., from 1.00% of sample S80-W4-50 to 0.09% of sample S80-W4-120. The N originated from the residual catalyst NH_3, which catalyzed the condensation of the

Table 5. Analysis Results of N_2 Adsorption for Selected Representative Samples with Different Storage Times

				NLDFT					
sample	storage time (day)	sample mass (mg)	S_{BET} (m^2/g)	model type	surface area (m^2/g)	pore width (nm)	pore volume (cc/g)	micropore volume (cc/g)	measuring time (h:min)
S80-E5+HW5-50	0	55.8	311.5	III	487.0	1.2	0.178	0.092	59:06
	50	65.9	30.0	III	26.8	3.8	0.039	0.002	15:15
S80-W10-50	0	62.9	344.3	III	564.0	1.1	0.186	0.108	41:08
	46	64.4	36.3	III	31.3	3.8	0.047	0.001	23:58
S80-HW10-50	0	51.9	351.8	III	555.3	1.1	0.195	0.105	36:26
	34	59.6	49.6	III	40.3	3.8	0.060		37:30
S80-W4-50+200	0	65.3	328.7	III	482.3	0.8	0.185	0.094	53:05
	13	61.6	323.2	III	494.0	0.8	0.185	0.092	61:39
	40	54.8	297.2	III	440.7	1.1	0.170	0.089	100:51

silanol groups, especially at higher temperatures. After centrifugation and decanting of the supernatant liquid, the wet product was placed in an oven to dry. From random close-sphere packing, the void fraction of the particles ranges from 36 to 44% depending on the packing density. Hence, the wet product actually contained large amounts of interparticle water and NH_3. When the wet product was direct dried at 120 or 200 °C, the water and NH_3 evaporated but over a certain amount of time. Condensation was promoted by the high temperature, which resulted in easy blocking of the pores due to the existence of a considerable amount of water and NH_3. After evaporation of the interparticle water, the Si-containing species in the water (see Figure 3) might become attached and condensed to the particle surfaces and pores, which also resulted in pore-blocking to a certain extent, and thus, the velocity of the N_2 molecules entering or diffusing in the pore channels became slow. However, for samples direct dried at 50 °C, the condensation of silanol groups should be much weaker due to the lower temperature, whereas interparticle water and NH_3 evaporated more slowly compared with that at 120 or 200 °C. Without efficient condensation, Si species should attach more loosely on the particle surfaces, and thus, the extent of pore-blocking is not significant. During outgassing, despite the high temperature, the pore-blocking was also not serious because most of the interparticle water and NH_3 had been removed compared with the wet product, and thus, the difference in the SSA between 120 and 200 °C outgassing is not obvious (see sample S80-W10-50 in Table 3). Therefore, for samples direct dried at 50 °C, the N_2 molecules could easily enter and diffuse in the pores, and thus, the measurement time was short.

Compared with selected complicated treatment processes for the synthesis of microporous and monodisperse silica spheres,[29] our water washing and controlled drying condition process appears quite simple. The drying temperature has been mentioned in previous studies, but the effect of the drying method was often overlooked. According to our experiment, the drying method (i.e., direct drying, heat drying, or vacuum) profoundly affected the results of N_2 adsorption. With the same slow measurement process, the adsorption volume of N_2 at 2.4×10^{-5} of p/p_0 is 14.7 cc/g for sample S80-W4-RT−120 (drying from room temperature to 120 °C), which is less than the 20.0 cc/g of sample S80-W4-120 (direct drying at 120 °C). The mechanism is the same as described above. The evaporation rate of NH_3 and water during the process of heating from room temperature to 120 °C was slow compared with that of direct drying at 120 °C, and thus, the condensation catalyzed by NH_3 intensified during the long evaporation time. Additionally, the pore-blocking was more serious than that under direct drying, and the presumed SSA (based on the adsorption volume at the same relative pressure) might be smaller than that under direct drying. We also treated the sample with direct vacuum drying at 50 °C (sample S80-W4-50V) and 200 °C (sample S80-W4-200V). The SSA of sample S80-W4-50V is much smaller (64.3 m^2/g) than that of sample S80-W4-50, perhaps because the micropores collapsed during the vacuum process because of capillary stress when water was extracted quickly.[30] The measurement time for sample S80-W4-200V was longer, and the adsorption volume (24.0 cc/g at 2.4×10^{-5} of p/p_0) is close to that of sample S80-W4-200 (22.6 cc/g at 2.4×10^{-5} of p/p_0), which suggests that, at such a high temperature, the influence of vacuum was not obvious.

3.4. Effect of Storage Time.

In our previous work,[26] many samples were stored for a long duration to wait for N_2 adsorption measurement because all samples were from one batch synthesis, and certain samples were measured for a long time (1 month). The pore-blocking mechanisms we proposed and the choice of water as a washing solvent were reasonable, as discussed in this work, although we realize that the storage time had a considerable impact on the N_2 adsorption results. Consequently, we tested the influence of the storage time on the SSA. For example, the SSA of sample S80-E5+HW5-50 shifted to 30.0 m^2/g from 311.5 m^2/g after 50 days of storage. Similar results were found for samples S80-W10-50 (from 344.3 to 36.3 m^2/g after 46 days of storage) and S80-HW10-50 (from 351.8 to 49.6 m^2/g after 34 days of storage) (see Table 5). The condensation of the silanol groups promoted by the NH_3 catalyst or high temperature during the synthesis or drying process should not be ignored during storage, even at ambient temperature, and especially in moist environments. Although the samples were stored in a desiccator with allochroic silica gel, they always contained some moisture that was trapped or adsorbed in the particles. Especially with samples dried at 50 °C, a considerable amount of residual water and NH_3 could lead to significant condensation that increased with storage time. Thus, the SSA of samples subjected to 50 °C drying decreased after a month of storage, indicating serious blocking of the pore channels or entrances. In this work, according to our preliminary examination, the SSA is not affected in 5 days, and thus, to ensure the accuracy of the data, all samples were stored for no more than 3 days prior to measurement.

A long storage time is certainly desirable in many applications, and thus, we searched for a better method for long-term storage of large-SSA Stöber silica. We selected direct drying at 50 °C for 2 h followed by direct drying at 200 °C for 2 h to treat the sample (denoted as sample S80-W4-50+200), and the effect of storage time was investigated. After 13 days of storage, the SSA, pore size, and measurement time were all similar to those found immediately after synthesis (0 day storage time in Table 5). After 40 days of storage, the measurement time exceeded 4 days, and the SSA decreased from >320 to 297 m^2/g. It appears that condensation occurred during the long storage period, but the extent of the pore-blocking was quite low due to the notably small amounts of residual moisture and NH_3 after additional direct drying at 200 °C. The SSA values of several samples with different storage times are shown in Figure 5. Lower temperature plus higher temperature direct drying is demonstrated as a more efficient method for the storage of Stöber silica. The reason for this result is the same as that discussed in section 3.3. A portion of the NH_3 and water evaporated at 50 °C such that the condensation during 200 °C drying was not obvious, and after 200 °C drying, both water and NH_3 were mostly removed, which led to slow condensation during storage.

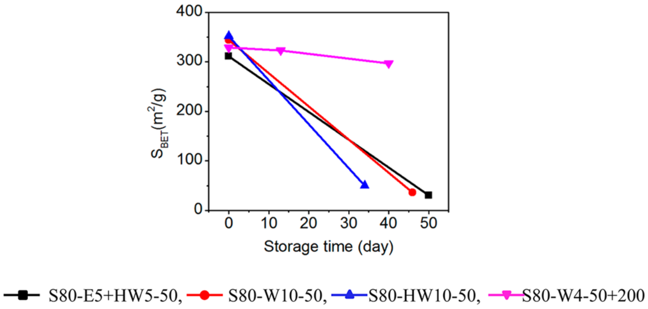

Figure 5. BET specific surface areas of samples with different storage times.

3.5. Effects of Other Factors.

In addition to the above significant factors, other factors also influence the process of N_2 adsorption, such as washing times and reaction time. In accordance with Figure 3, the extent of pore-blocking might be related to the washing times. For example, the SSA of sample S80-W10-120–200 (10 washes) is 315.6 m^2/g, and the measurement time is approximately 78 h. The measurement time for sample S80-W4-120–200 (4 washes) was longer, and after 4 days of measurement, the p/p_0 only reached 2.4×10^{-5}. We believe 10 washes could clear the oligomers and monomers more completely than 4 washes, and thus, during high temperature drying, the pore-blocking of sample S80-W10-120–200 caused by condensation or residual Si species was less significant than that of sample S80-W4-120–200. Although the SSA of the sample with 2 washes and direct drying at 50 °C is similarly large and the measurement was as quick as that of sample S80-W10-50, additional washing times are suggested to clear the pore entrances or channels more thoroughly for further application.

To investigate the effect of the reaction time, 80 and 180 min reaction times were compared. The results of the different reaction times were influenced by the drying conditions. Under 50 °C direct drying, the difference between the SSAs of sample S80-W4-50 and sample S180-W4-50 is not obvious in that both SSAs are large and the measurement times are short, but for samples with 120 °C direct drying or drying from room temperature to 120 °C, the differences are noticeable. Although the measurements of these samples were not finished, the adsorption volume of N_2 at the same relative pressure for sample S80-W4-RT–120 is much larger (14.7 cc/g at 2.4×10^{-5}) than that of sample S180-W4-RT–120 (1.8 cc/g at 2.4×10^{-5}). According to the aggregation plus monomer addition growth model, the longer the reaction time, the more dense the surface of the Stöber silica particles, and thus, the pore-blocking caused by condensation can be intensified on denser particle surfaces.

4. CONCLUSIONS

The multiple factors that influence the pore characteristics of Stöber silica were investigated. The measurement time was shortened from 1 month in the previous work to 2–3 days for large SSA samples. Although these factors were examined in previous studies, the key point in the acquisition of Stöber silica with large SSA and short measurement is that water washing must be combined with a lower drying temperature (without vacuum) and a short storage time. The pore-blocking mechanisms and particle growth model are strengthened by strong evidence (ICP-OES and TEM). The effect of storage time was often unnoticed in many investigations, but it significantly influences the N_2 adsorption through condensation of silanol groups. The drying method also affects the extent of pore-blocking by the same condensation mechanisms. The extent of pore-blocking determines the entry and diffusion velocity of nitrogen molecules in the particles and is reflected by the measurement time, which offers a reference measurement for similar microporous materials. In the future, the internal subtle microporous structure and the discrepant SSA values of Stöber silica in the literature are expected to be understood, which will provide a sound basis for its continued use in diverse applications and fundamental research.

■ ASSOCIATED CONTENT

Ⓢ Supporting Information

The Supporting Information is available free of charge on the ACS Publications website at DOI: 10.1021/acs.langmuir.6b02472.

Additional gas adsorption isotherm, infrared transmission spectra, and equations for selected representative samples and processes (PDF)

■ AUTHOR INFORMATION

Corresponding Author

*E-mail: wanquan@vip.gyig.ac.cn.

Notes

The authors declare no competing financial interest.

■ ACKNOWLEDGMENTS

Q.W. gratefully acknowledges support of this work by the Chinese Academy of Sciences ("Hundred Talents Program"), the National Natural Science Foundation of China (41473064), and the State Key Laboratory of Ore Deposit Geochemistry (SKLODG-ZY125-09).

■ REFERENCES

(1) Stöber, W.; Fink, A.; Bohn, E. Controlled Growth of Monodisperse Silica Spheres in the Micron Size Range. *J. Colloid Interface Sci.* **1968**, *26* (1), 62–69.

(2) Wong, Y. J.; Zhu, L.; Teo, W. S.; Tan, Y. W.; Yang, Y.; Wang, C.; Chen, H. Revisiting the Stöber Method: Inhomogeneity in Silica Shells. *J. Am. Chem. Soc.* **2011**, *133* (30), 11422–11425.

(3) Cho, S.-H.; Park, S. Y.; Kim, C.; Choi, P.-P.; Park, J.-K. Stabilization of Monodispersed Spherical Silica Particles and Their

Alignment with Reduced Crack Density. *Colloids Surf., A* **2014**, *441*, 354−359.

(4) Diedrich, T.; Dybowska, A.; Schott, J.; Valsarni-Jones, E.; Oelkers, E. H. The Dissolution Rates of SiO2 Nanoparticles As a Function of Particle Size. *Environ. Sci. Technol.* **2012**, *46* (9), 4909−4915.

(5) Mueller, R.; Kammler, H. K.; Wegner, K.; Pratsinis, S. E. OH Surface Density of SiO_2 and TiO_2 by Thermogravimetric Analysis. *Langmuir* **2003**, *19* (1), 160−165.

(6) Kim, J. M.; Chang, S. M.; Kong, S. M.; Kim, K. S.; Kim, J.; Kim, W. S. Control of Hydroxyl Group Content in Silica Particle Synthesized by the Sol-Precipitation Process. *Ceram. Int.* **2009**, *35* (3), 1015−1019.

(7) Bogush, G. H.; Tracy, M. A.; Zukoski, C. F. Preparation of Monodisperse Silica Particles Control of Size and Mass Fraction. *J. Non-Cryst. Solids* **1988**, *104*, 95−106.

(8) Wang, H.-C.; Wu, C.-Y.; Chung, C.-C.; Lai, M.-H.; Chung, T.-W. Analysis of Parameters and Interaction between Parameters in Preparation of Uniform Silicon Dioxide Nanoparticles using Response Surface Methodology. *Ind. Eng. Chem. Res.* **2006**, *45* (24), 8043−8048.

(9) Hartlen, K. D.; Athanasopoulos, A. P. T.; Kitaev, V. *Langmuir* **2008**, *24* (5), 1714−1720.

(10) Sumper, M.; Lorenz, S.; Brunner, E. *Angew. Chem., Int. Ed.* **2003**, *42* (42), 5192−5195.

(11) Wang, Y. F. Nanogeochemistry: Nanostructures, Emergent Properties and Their Control on Geochemical Reactions and Mass Transfers. *Chem. Geol.* **2014**, *378−379*, 1−23.

(12) Hochella, M. F. Nanogeoscience: from Origins to Cutting-edge Applications. *Elements* **2008**, *4*, 373−379.

(13) Wu, D.; Navrotsky, A. Small Molecule-Silica Interactions in Porous Silica Structures. *Geochim. Cosmochim. Acta* **2013**, *109*, 38−50.

(14) Wu, D.; Hwang, S.-J.; Zones, S. I.; Navrotsky, A. Guest-Host Interactions of a Rigid Organic Molecule in Porous Silica Frameworks. *Proc. Natl. Acad. Sci. U. S. A.* **2014**, *111* (5), 1720−1725.

(15) Labrosse, A.; Burneau, A. Characterization of Porosity of Ammonia Catalysed Alkoxysilane Silica. *J. Non-Cryst. Solids* **1997**, *221* (2−3), 107−124.

(16) Balas, F.; Rodriguez-Delgado, M.; Otero-Arean, C.; Conde, F.; Matesanz, E.; Esquivias, L.; Ramirez-Castellanos, J.; Gonzalez-Calbet, J.; Vallet-Regi, M. Structural Characterization of Nanosized Silica Spheres. *Solid State Sci.* **2007**, *9* (5), 351−356.

(17) Szekeres, M.; Toth, J.; Dekany, I. Specific Surface Area of Stöber Silica Determined by Various Experimental Methods. *Langmuir* **2002**, *18* (7), 2678−2685.

(18) Howard, A.; Khdary, N. Spray Synthesis of Monodisperse Sub-Micron Spherical Silica Particles. *Mater. Lett.* **2007**, *61* (8−9), 1951−1954.

(19) Davis, P. J.; Deshpande, R.; Smith, D. M.; Brinker, C. J.; Assink, R. A. Pore Structure Evolution in Silica Gel during Aging/Drying. IV. Varying Pore Fluid pH. *J. Non-Cryst. Solids* **1994**, *167* (3), 295−306.

(20) Peng, L.; Qisui, W.; Xi, L.; Chaocan, Z. Investigation of the States of Water and OH Groups on the Surface of Silica. *Colloids Surf., A* **2009**, *334* (1−3), 112−115.

(21) Filipovic, R.; Obrenovic, Z.; Stijepovic, I.; Nikolic, L. M.; Srdic, V. V. Synthesis of Mesoporous Silica Particles with Controlled Pore Structure. *Ceram. Int.* **2009**, *35* (8), 3347−3353.

(22) Dekany, I.; Nemeth, J.; Szekeres, M.; Schoonheydt, R. Surfacial, Liquid Sorption and Monolayer-Forming Properties of Hydrophilic and Hydrophobic Stöber Silica Particles. *Colloid Polym. Sci.* **2003**, *282* (1), 1−6.

(23) Wan, Q.; Ramsey, C.; Baran, G. Thermal Pretreatment of Silica Composite Filler Materials. *J. Therm. Anal. Calorim.* **2010**, *99* (1), 237−243.

(24) Wells, J. D.; Koopal, L. K.; Keizer, A.d. Monodisperse, Nonporous, Spherical Silica Particles. *Colloids Surf., A* **2000**, *166*, 171−176.

(25) Zhuravlev, L. T. The Surface Chemistry of Amorphous Silica. Zhuravlev Model. *Colloids Surf., A* **2000**, *173* (1−3), 1−38.

(26) Li, S. S.; Wan, Q.; Qin, Z. H.; Fu, Y. H.; Gu, Y. T. Understanding Stöber Silica's Pore Characteristics Measured by Gas Adsorption. *Langmuir* **2015**, *31* (2), 824−832.

(27) Giesche, H. Synthesis of Monodispersed Silica Powders I. Particle Properties and Reaction Kinetics. *J. Eur. Ceram. Soc.* **1994**, *14*, 189−204.

(28) Iler, R. K. *The Chemistry of Silica: Solubility, Polymerization, Colloid and Surface Properties*; Wiley-Interscience: New York, 1979.

(29) Bazula, P. A.; Arnal, P. M.; Galeano, C.; Zibrowius, B.; Schmidt, W.; Schuth, F. Highly Microporous Monodisperse Silica Spheres Synthesized by the Stöber Process. *Microporous Mesoporous Mater.* **2014**, *200*, 317−325.

(30) López Pérez, L.; van Eck, E. R. H.; Melian-Cabrera, I. On the Hydrothermal Stability of MCM-41. Evidence of Capillary Tension-induced Effects. *Microporous Mesoporous Mater.* **2016**, *220*, 88−98.